10

OFFSHORE TECHNOLOGY CONFERENCE

OTC 4437

On the Low-Frequency Surge Motions of Vessels Moored in High Seas

by J.E.W. Wichers, *Netherlands Ship Model Basin*

ABSTRACT

Moored floating structures for drilling, production and/or storage purposes are being installed in ever increasing water depths and in areas where the environmental conditions are also more severe. As a result of the increased water depth, the elasticity of the mooring system increases.

With the increase in the elasticity of the mooring, the low-frequency horizontal motions induced by low-frequency second-order wave drift forces also become larger. These low-frequency motion components completely dominate the horizontal motions and as a consequency also the mooring forces. Therefore it is necessary to investigate the low-frequency motions for those situations where greater water depths and more extreme sea conditions occur.

In this paper, results are given of an investigation into the low-frequency surge motions of a large storage tanker moored in a linear system in deep water subject to high head seas. Results of model tests are compared with results of computations. For the computations the term "wave damping" has been introduced. It will be shown that the wave damping significantly influences the low-frequency surge motions. A good agreement between the measured and computed low-frequency surge motions has been found.

INTRODUCTION

Floating structures moored at sea are subjected to forces that tend to shift them from their desired position. For a given vessel the motions depend both on the mooring system and on the external forces acting on the vessel. The forces on the vessel caused by an irregular sea are of an irregular nature and may be split into two parts:

- first-order oscillatory forces with wave frequency, and
- second-order, slowly varying forces with frequencies much lower than the wave frequency.

References and illustrations at end of paper

The first-order oscillatory wave forces on a vessel cause the well-known ship motions, with frequencies equal to the frequencies present in the spectrum of the irregular waves.

The second-order wave forces, better known as the wave drift forces, have been shown to be proportional to the square of the wave height (ref. [1], [2] and [3]). These forces, though small in magnitude, are the cause of the low-frequency, large-amplitude, horizontal motions of vessels moored at sea.

An example of these low-frequency, large-amplitude surge motions in irregular head seas, as measured on a model of a 200,000 DWT VLCC moored in an ideal mooring system, is shown in Figure 1. The results are given as full scale values. The stiffness of this ideal linear mooring system approximately corresponds to the stiffness of single anchor leg moorings usually applied in deep water. The head waves shown in the recording of Figure 1 corresponds to high seas. From Figure 1 it can be seen that the high-frequency surge motions are negligible small, which means that the surge motions are dominated by the low frequency surge motions.

For this paper computations and model tests were carried out for a series of wave spectra to study the low-frequency motions of a fully loaded 200,000 DWT storage tanker in head seas and for two linear mooring systems.

The series of wave spectra had the following characteristics:

Wave spectrum No.	Significant wave height $4\sqrt{m_{\zeta 0}}$ (m)	Significant wave height $\zeta_{w1/3}$ (m)	Mean period $2\pi(m_{\zeta 0}/m_{\zeta 1})$ (sec.)
1	12.5	12.33	14.0
2	9.4	9.45	13.7
3	7.5	7.61	13.6
4	5.1	5.16	13.3
5	12.5	-	12.0
6	9.8	9.85	12.0
7	6.1	6.01	11.4
8	4.9	4.86	11.1

For the computation of the low-frequency surge motion not only the still water damping but also the damping caused by the waves at the resonant surge motions of the tanker has been taken into account (see ref. [4]). From ref. [4] it was found that the wave damping coefficient is a time-dependent coefficient.

For the computations two techniques were applied:

- time domain simulation (applied to wave spectrum No. 1).
- frequency domain technique (applied to wave spectrum No. 1 through 8).

The time domain simulation shows that the time-dependent wave damping coefficient can be replaced by a constant wave damping coefficient. This means that the computations can be carried out in the frequency domain.

In some of the wave spectra model tests were carried out to compare the measured results with the computed results of the surge motions. In wave spectrum No. 1 also the wave drift forces were measured to verify the computed wave drift forces in high seas.

From the results obtained by the time domain simulation and the frequency domain technique it was concluded that the wave damping significantly influences the low-frequency motions.

In the next sections the model experiments will be described followed by the description of the wave damping phenomenon. The computation techniques will be elucidated and finally the measured and computed results will be compared.

MODEL EXPERIMENTS

Test set-up

The model tests in the irregular waves were carried out in the Seakeeping Laboratory of the Netherlands Ship Model Basin having a water depth of 2.5 m, a length of 100 m, and a width of 24 m. Use was made of a model of a fully loaded 200,000 DWT storage tanker (scale 1:82.5) with a block coefficient of 0.85. The particulars of the vessel are given in Table 1. The body plan is shown in Figure 2. For the tests two linear mooring systems were employed for the tanker, the spring constants C_x were 13.60 and 53.72 ton.m^{-1}. The test set-up of the mooring arrangement for the model experiments is shown in Figure 3. This test set-up including the model corresponds exactly to the set-up as used in ref. [4], in which the experimentally determined wave damping has been given.

Measurements

The wave spectra No. 1, 2, 3, 4, 6, 7 and 8 were adjusted in the basin. Figure 4 shows the wave spectral density functions. Each sea state was prepared for a test duration of 150 minutes prototype scale. During the tests the surge (x), heave (z) and pitch (θ)-motions were measured. The surge and heave motions were measured in the centre of gravity (C.o.G.) by means of an optical tracking device.

The pitch motions were measured by means of a gyroscope. The sign-convention is given in Figure 3. Prior to the tests in waves surge extinction tests were performed in still water, to measure the natural periods and still water low-frequency damping coefficients. The data are given in Table 2.

Data analysis

The irregular signals of the motions were recorded on magnitic tape and subjected to statistical analysis. The statistical analysis performed on the various motions are:

1. Mean value: $\bar{u}$

$$\bar{u} = \frac{1}{N} \sum_{n=1}^{n=N} u_n \quad (N \text{ is number of samples})$$

2. Root-mean square value: σ_u

$$\sigma_u = \sqrt{\frac{1}{N} \sum_{n=1}^{n=N} (u_n - \bar{u})^2}$$

3. Maximum value: $u_{a\ max.}^{+}$

   Highest peak-to-zero value.

4. Minimum value: $u_{a\ max.}^{-}$

   Highest zero-to-trough value.

5. Maximum double amplitude: $2u_{a\ max.}$

   This is the maximum crest-to-trough value.

6. Significant peak value: $\tilde{u}_{a1/3}^{+}$

   This is the mean of the one-third highest crest-to-zero values.

7. Significant trough value: $\tilde{u}_{a1/3}^{-}$

   This is the mean of the one-third highest zero-to-trough values.

8. Significant double amplitude: $2\tilde{u}_{a1/3}$

   This is the mean of the highest one-third crest-to-trough values.

9. Number of oscillations: N_u

   This is the total number of oscillations in the record.

Review of test program

The model experiments were conducted for the wave spectra No. 1, 2, 6, 7 and 8. A review of the test program is given in Table 3. Some typical results of the motion measurements are given in Tables 3 and 6 and in Figures 5, 6 and 12.

Wave drift force measurement

Besides motions wave drift forces were measured on the tanker in wave spectrum No. 1. To measure the low-frequency longitudinal wave drift forces the vessel was moored by means of a stiff mooring system in which transducers were inserted. The linear spring

constant was $C_x = 568$ ton.m^{-1}. The wave drift forces were recorded on magnetic tape. The spectral density of the measured wave drift force for the frequency range concerned is shown in Figure 11.

THE PHENOMENON WAVE DAMPING

Still water damping

To compute the low-frequency surge motions of a moored vessel the equations of motion must be drawn up and solved. The low-frequency (oscillatory) surge motions of the moored vessel in head waves will be excited by the wave drift forces. The equation of the low-frequency motion in the longitudinal (x) direction reads:

$$(m + a_{xx})\ddot{x} + b_{xx}.\dot{x} + C_x = F_x(t) \quad \ldots\ldots (1)$$

In this equation C_x represents the spring constant of the mooring system. To solve the equation the added mass of the vessel a_{xx} and the hydrodynamic damping h_{xx} have to be known. Both coefficients are dependent on the frequency of motion. The damping of the vessel in still water consists of the following parts:

- potential damping (energy loss due to the radiated waves caused by the oscillating vessel);
- viscous damping (energy loss caused by friction).

At low frequencies the potential damping is negligibly small; therefore the still water damping will be dominated by viscous damping. Taking into account the still water damping only, equation (1) can be written as follows:

$$(m + a_{xx}(\omega_x))\ddot{x} + b_{oxx}(\omega_x).\dot{x} + C_x.x = F_x(t) \quad \ldots\ldots\ldots\ldots\ldots\ldots (2)$$

in which:

$b_{oxx}(\omega_x)$ = still water damping coefficient at the natural frequency ω_x.

$a_{xx}(\omega_x)$ = added mass coefficient at the natural frequency ω_x.

Wave damping

Actually, however, the vessel is moored in waves. In ref. [4] the influence of the waves on the low-frequency hydrodynamic coefficients of a 200,000 DWT VLCC in deep water (206 m) is given. An example of the experimentally determined damping coefficients in still water and in regular waves is given in Figure 7. From this example it can be derived that:

- the damping coefficient in still water is approximately linearly proportional to the surge velocity.
- the damping coefficient in regular waves is approximately linearly proportional to the surge velocity.
- due to the linearity the principle of superposition of damping may be assumed.
- using the principle of superposition the contribution of the damping caused by the waves only can be determined: This is called the wave damping.
- The wave damping seems to be linearly proportional to the square of the wave height.

Moreover, in ref. [4], it has been shown that the value of the wave damping is dependent on the wave frequency. Because the wave damping is dependent on the wave frequency and linearly proportional to the square of the wave height, the wave damping can be treated as a quadratic transfer function. Further it seems that the wave damping is independent of the frequency of the resonant surge motion.

As is shown in Figure 7 and in ref. [4] it appears that the total damping in waves can be split up into the following components:

- the still water low-frequency damping,
- the wave damping.

By taking into account the wave damping equation (2) can be modified as follows:

$$[m + a_{xx}(\omega_x)]\ddot{x} + b_{oxx}(\omega_x).\dot{x} + b_{1xx}(t).\dot{x} + C_x.x = F_x(t) \quad \ldots\ldots\ldots\ldots (3)$$

in which:

$b_{1xx}(t)$ is called the wave damping coefficient.

Equation (3) is a second-order linear differential equation with a time-dependent coefficient. Because the model and the test set-up were taken the same as used in ref. [4] the results derived from ref. [4] can be applied to the present computations. The main results, being the low-frequency still water damping and the quadratic transfer function of the wave damping are shown in the Figures 8 and 9.

TIME DOMAIN SIMULATION

Time domain simulation of the wave damping coefficient

Using the quadratic transfer function of the wave damping the wave damping coefficient in the time domain can be determined when the square of the wave envelope and the wave frequency of the wave train are known. For this purpose the following method is applied. From the time-records of the waves $\zeta(t)$ adjusted in the basin the time-records of the instantaneous wave frequency $\omega(t)$ and the instantaneous wave envelope $A(t)$ were determined by using Hilbert transforms.

The Hilbert transform of a signal f(t) is defined as (see ref. [5]):

$$f_H(t) = \frac{1}{\pi} \int_{-\infty}^{+\infty} \frac{f(\tau)}{t-\tau}\, d\tau \quad \ldots\ldots\ldots\ldots (4)$$

The frequency characteristic of a Hilbert filter (transfer function) is as follows:

$$H(\omega) = -i \text{ sign } (\omega) = \begin{cases} -i & (\omega > 0) \\ 0 & (\omega = 0) \\ i & (\omega < 0) \end{cases} \quad \ldots\ldots (5)$$

From equation (5) it follows that:

$$F_H(\omega) = F(\omega).H(\omega) = -i\, F(\omega)\, \text{sign}(\omega) \quad \ldots\ldots (6)$$

where:

$F(\omega)$ = Fourier transform of f(t)
$F_H(\omega)$ = Fourier transform of $f_H(t)$

Thus the Hilbert transform of a signal is found by passing it through an ideal 90° phase shifter. Now considering the signal of an irregular wave we will have:

$$\zeta(t) = A(t) \cos \omega(t) \quad \ldots\ldots\ldots\ldots (7)$$

Then it follows that:

$$A^2(t) = \zeta^2(t) + \zeta_H^2(t) \quad \ldots\ldots\ldots\ldots (8)$$

and:

$$\omega(t) = \arctan \left[\frac{\zeta_H(t)}{\zeta(t)}\right] \quad \ldots\ldots\ldots\ldots (9)$$

Considering the quadratic transfer function of the wave damping as shown in Figure 9, the wave damping coefficient in a wave train can be formulated as follows:

$$b_{1xx}(t) = b'_{1xx}\,(\omega(t)).A^2(t) \quad \ldots\ldots (10)$$

Using equations (8), (9) and (10) based on the time record of the adjusted waves $\zeta(t)$ of wave spectrum No. 1 in Figure 10 an example is given of computed time records of:

- wave frequency $\omega(t)$
- wave envelope $A(t)$
- square of wave envelope $A^2(t)$
- wave damping coefficient

Time domain computation of the wave drift forces

The quadratic transfer function of the wave drift forces for the tanker in head waves was computed according to the direct pressure integration method (see ref. [3]). The results are shown in Table 4. The time history of the wave drift force was obtained by applying a quadratic impulse response function to the record of the measured wave train. This quadratic impulse response function technique was first applied by Dalzell (see ref. [6]) to the problem of wave drift forces. By means of Fourier transform the quadratic impulse response function can be written as follows:

$$g(\tau_1,\tau_2) = \frac{1}{2\pi^2} \int_{-\infty}^{+\infty}\int_{-\infty}^{+\infty} G(\omega_1,\omega_2).\exp(i\omega_1\tau_1 + - i\omega_2\tau_2)\, d\omega_1\, d\omega_2 \quad \ldots\ldots (11)$$

in which:

$G(\omega_1,\omega_2)$ = complex quadratic transfer function
$= P(\omega_1,\omega_2) + iQ(\omega_1,\omega_2)$

and:

$P(\omega_1,\omega_2)$, $Q(\omega_1,\omega_2)$ = in-phase and out-of-phase components of the quadratic transfer function as given in Table 4.

Using the record of the adjusted waves $\zeta(t)$ the time domain simulation of the wave drift force can be written as:

$$F(t) = \int_{-\infty}^{\infty}\int_{-\infty}^{\infty} g(\tau_1,\tau_2)\,\zeta(t-\tau_1)\,\zeta(t-\tau_2)\,. \; . d\tau_1.d\tau_2 \quad \ldots\ldots (12)$$

For a detailed description of the formulation see ref. [7]. Using the time-record of the adjusted waves of spectrum No. 1, the longitudinal wave drift forces were computed. A part of the time domain record of the wave drift force is shown on the plot of Figure 10.

Time domain simulation of the surge motion

Using equation (2) and (3) respectively without and with wave damping the low-frequency surge motions in the time domain were computed. The computations only concern the highest sea state (wave spectrum No. 1) and for the tanker, with a spring constant $C_x = 13.6$ ton.m^{-1}. The following input data were used:

- the experimentably determined data of the system given in Table 2.

and the time-records of:

- the computed wave damping coefficient,
- the computed wave drift force,
- the measured wave drift force.

Results time domain simulation

- Wave damping
  Of each of the adjusted wave trains in the basin (wave spectra No. 1, 2, 3, 4, 6, 7 and 8) the time-records of the wave damping coefficients were computed according to equation (10) and statistically analyzed. The mean values are shown in Table 5.

- Wave drift forces
  The spectral density of the theoretical wave drift forces determined in wave spectrum No. 1 according to equation (12) is presented in Figure 11. The spectral density of the wave drift force measured in wave spectrum No. 1 is also given in Figure 11. The spectral density is given for the frequency range concerned.

- Surge motion
  The time domain simulations of the surge motion were statistically analyzed. Some typical statistical data of the simulation are shown in Table 6.

SIMPLIFICATION OF THE WAVE DAMPING COEFFICIENT

In Figure 10 it can be seen that the wave damping coefficient $b_{1xx}(t)$ consists of a mean and an oscillating part. In order to clearly distinguish these two parts the formulation of a regular wave group consisting of two regular waves with amplitudes ζ_1 and ζ_2, wave frequencies ω_1 and ω_2, wave numbers k_1 and k_2 and phases ε_1 and ε_2 respectively, will be applied to the equation of surge motion. The wave group can be written as follows:

$$\zeta_{tot}(t) = A(t)\,\sin(\bar{\omega}\,t - \bar{k}x + \bar{\varepsilon}) \quad \ldots\ldots (13)$$

while:

$A(t)$ = wave group envelope

$$= [\zeta_1^2 + \zeta_2^2 + 2\zeta_1.\zeta_2\,\cos\{\Delta\omega.t - \Delta k.x + \Delta\varepsilon\}] \quad \ldots\ldots\ldots\ldots (14)$$

while: $\bar{\omega} = \frac{\omega_1 + \omega_2}{2}$, $\bar{k} = \frac{k_1 + k_2}{2}$, $\bar{\varepsilon} = \frac{\varepsilon_1 + \varepsilon_2}{2}$

and : $\Delta\omega = \omega_1 - \omega_2$, $\Delta k = k_1 - k_2$, $\Delta\varepsilon = \varepsilon_1 - \varepsilon_2$

Considering the resonant surge motion $\Delta\omega = \sqrt{\frac{C_x}{m_{xx}}}$, x=0 and $\varepsilon_1 = \varepsilon_2$ equation (3) can be written as:

$$m_{xx}.\ddot{x} + b_{oxx}.\dot{x} + b'_{1xx}(\bar{\omega}).A^2(t).\dot{x} + C_x.x = F_d + F_a \cos \Delta\omega t \quad \ldots\ldots\ldots\ldots (15)$$

in which:

F_d = mean wave drift force of the wave group.
F_a = oscillating part of the wave drift force of the wave group.

or:

$$m_{xx}.\ddot{x} + b_{oxx}.\dot{x} + \underbrace{b'_{1xx}(\bar{\omega})\left[\zeta_1^2 + \zeta_2^2\right]\dot{x}}_{\text{mean wave damping force}} + \underbrace{2b'_{1xx}(\bar{\omega})\,\zeta_1 . \zeta_2 . \cos \Delta\omega t . \dot{x}}_{\text{oscillating wave damping force}} + C_x . x = F_d + F_a \cos \Delta\omega t \quad \ldots\ldots\ldots\ldots (16)$$

It can be proven that for systems with a low damping the contribution of the oscillating wave damping force to the response of the surge motion is negligibly small. This statement holds true for both a regular wave group and for an irregular wave group (wave spectrum). The still water damping and the mean wave damping coefficient will dominate the magnitude of the surge motion. As a consequence equation (16) can be written in a simplified form:

$$m_{xx}.\ddot{x} + b_{oxx}.\dot{x} + b'_{1xx}(\bar{\omega})\left[\zeta_1^2 + \zeta_2^2\right]\dot{x} + C_x.x = F_d + F_a \cos \Delta\omega t \quad \ldots\ldots\ldots\ldots (17)$$

As an illustration for an irregular sea (wave spectrum No. 1) the time domain simulation of the surge motion taking into account the still water damping coefficient (see Table 2) and the mean wave damping coefficient (see Table 5) was carried out. The results are shown in Table 6. The results hardly deviate from the results obtained from the computations using the complete damping formulation.

FREQUENCY DOMAIN TECHNIQUE

Wave damping coefficient

The mean wave damping force as given in equation (17) reads:

$$b'_{1xx}(\bar{\omega})\left[\zeta_1^2 + \zeta_2^2\right].\dot{x} \quad \ldots\ldots\ldots (18)$$

or using the quadratic transfer function given in Figure 9:

$$\left\{\frac{b_{1xx}}{\zeta_a^2}(\omega_1).\zeta_1^2 + \frac{b_{1xx}}{\zeta_a^2}(\omega_2).\zeta_2^2\right\}.\dot{x} \quad \ldots\ldots (19)$$

In an irregular sea with N wave components we obtain:

$$\left\{\sum_{i=1}^{N} \zeta_i^2 . \frac{b_{1xx}}{\zeta_a^2}(\omega_i)\right\}.\dot{x} \quad \ldots\ldots\ldots (20)$$

or in spectral notation:

$$\left\{2\int_0^\infty S_\zeta(\omega)\,\frac{b_{1xx}}{\zeta_a^2}(\omega)\,d\omega\right\}.\dot{x} \quad \ldots\ldots (21)$$

in which:

$S_\zeta(\omega)$ = spectral density of the sea state applied.

Equation (21) will be denoted as:

$$\overline{b_{1xx}} . \dot{x} \quad \ldots\ldots\ldots\ldots\ldots (22)$$

in which:

$\overline{b_{1xx}}$ = mean wave damping coefficient.

Using the mean wave damping coefficient equation (3) can be written as:

$$m_{xx}.\ddot{x} + (b_{oxx} + \overline{b_{1xx}})\dot{x} + C_x.x = F_x(t) \quad \ldots\ldots\ldots\ldots\ldots (23)$$

Wave drift forces

The spectral density of the wave drift forces in an irregular sea state with the spectral density $S_\zeta(\omega)$ can be written as (see ref. [3]):

$$S_{F_x}(\mu) = 8\int_0^\infty S_\zeta(\omega).S_\zeta(\omega+\mu)\left[T(\omega,\omega+\mu)\right]^2 d\omega \quad \ldots\ldots\ldots\ldots\ldots (24)$$

in which:

μ = frequency of low-frequency part of the second-order forces
$T(\omega,\omega+\mu)$ = amplitudes of the quadratic transfer function of the wave drift force dependent on ω and $\omega+\mu$ as is given in Table 4.

Using the spectral density of wave spectrum No. 1 the spectral density of the longitudinal wave drift force according to equation (24) has been shown in Figure 11.

Surge motion response

Since the equation of motion (23) is simplified into a linear form, the low-frequency surge motion may be determined in the frequency domain. The root-mean square value of the low-frequency surge motion σ_x follows from:

$$\sigma_x^2 = \int_0^\infty S_{F_x}(\mu) . \left\{\frac{x_a}{F_a}(\mu)\right\}^2 . d\mu \quad \ldots\ldots (25)$$

where:

$S_{F_x}(\mu)$ = spectral density of the longitudinal wave drift force
$\frac{x_a}{F_a}(\mu)$ = surge amplitude per unit longitudinal wave drift force

$$= \frac{1}{\sqrt{(C_x - m_{xx}\mu^2)^2 + (b_{oxx} + \overline{b_{1xx}})^2 \mu^2}} \quad \ldots\ldots\ldots\ldots\ldots\ldots (26)$$

For systems which have a low damping, the response of the surge motion at the natural frequency μ_e will dominate (see Figure 6). In such cases equation (25) becomes:

$$\sigma_x^2 \simeq S_{F_x}(\mu_e) \cdot \int_0^\infty \left\{\frac{x_a}{F_a}(\mu)\right\}^2 d\mu \quad \ldots\ldots (27)$$

which, taking equation (25) into account, becomes:

$$\sigma_x^2 \simeq \frac{\pi}{2(b_{oxx} + \overline{b_{1xx}})\, C_x} \cdot S_{F_x}(\mu_e) \quad \ldots\ldots (28)$$

where $\mu_e = \sqrt{\frac{C_x}{m_{xx}}}$ = natural frequency of the system in rad./sec.

and $S_{F_x}(\mu_e)$ = spectral density of the wave drift force at frequency μ_e.

Results frequency domain

The frequency domain computations have been carried out for the tanker with the linear spring constant $C_x = 13.60$ ton.m^{-1} for all wave spectra as is shown in Figure 4; for the tanker with the linear spring constant $C_x = 52.73$ ton.m^{-1} wave spectra No. 5, 6, 7 and 8 were applied.

The computations on the surge motion were performed both for the still water damping coefficient only and the still water damping plus the mean wave damping coefficient.

The results of the computed spectral densities of the wave drift forces $S_{F_x}(\mu_e)$ according to equation (24) are shown in Table 7.

The mean wave damping coefficients $\overline{b_{1xx}}$ calculated according to equation (21) are given in Table 5.

The results of the calculated root-mean square values of the surge motions with and without the mean wave damping coefficient are shown in Table 3 and in Figure 12.

COMPARISON OF EXPERIMENTAL AND COMPUTED RESULTS

- Computed/measured wave drift forces
  The spectral densities of the wave drift forces computed according to the time and frequency domain formulation and the measured wave drift force are shown in Figure 11. All wave drift forces concern wave spectrum No. 1. For the natural frequency of the system $\mu_e = 0.023$ rad./sec. the spectral density of the time domain computed wave drift force is somewhat larger than the frequency domain computed and the measured wave drift forces; it seems that for wave spectrum No. 1 the spectral density $S_{F_x}(\mu_e)$ computed in the time domain is not significantly influenced by non-linearities of the high waves.

- Mean wave damping coefficient time/frequency domain
  The mean wave damping coefficients computed according to the time and frequency domain formulation are shown in Table 5. The results agree well.

- Measured and computed surge motion/time domain
  Some typical statistical results of the measured and computed low-frequency surge motions are given in Table 6. The computed results are given with and without wave damping. For the investigated wave spectra the computed results without wave damping are significantly overestimated with regard to the measured values. With wave damping the results agree well with the measured data. In case the mean (constant) wave damping coefficient was applied to the time domain computation hardly any deviation was found with regard to the results of the time domain computation using the time-dependent wave damping coefficient.

- Measured and frequency domain computed σ_x
  In Table 3 and in Figure 12 the measured and the frequency domain computed root-mean square values σ_x are given. The computed results are given with and without the mean wave damping coefficient. For the investigated spectra the results without the mean wave damping coefficient are significantly overestimated with regard to the measured values. With the mean wave damping coefficient a good agreement was found.

CONCLUSIONS

In the present study experimentally and theoretically determined low-frequency surge motions of a moored tanker in irregular head seas have been compared.

In drawing up the equation of motions, using the low-frequency still water damping coefficient only, the solved surge motions appear to be significantly overestimated.

Waves seem to contribute an additional damping superimposed on the low-frequency still water damping. The wave damping seems to be dependent on the wave frequency and linearly proportional to the square of the wave height.

Taking into account the quadratic transfer function of the wave damping in the equations of motion the solved surge motions were significantly influenced. The computed results correspond with the measured data.

Time domain simulations show that the time-dependent wave damping coefficient can be simplified into a mean (constant) wave damping coefficient. For each wave spectrum the mean wave damping coefficient can be calculated. As a consequence the low-frequency motion response can be computed in the frequency domain.

Applying the still water damping coefficient plus the mean wave damping coefficient in order to compute the low-frequency surge motions a good agreement is found with the measured surge motions.

Additional physical and theoretical investigations are required to understand the phenomenon "wave damping".

NOMENCLATURE

A = wave group envelope

a_{xx} = added mass in x-direction

B = breadth of vessel

b = damping coefficient

b_{oxx} = low-frequency still water damping coefficient in x-direction

b_{1xx} = wave damping coefficient in x-direction

b'_{1xx} = longitudinal quadratic transfer function of wave damping = b_{1xx}/ζ_a^2

$\overline{b_{1xx}}$ = mean wave damping coefficient

C_x = spring constant in x-direction

F_x = low-frequency wave drift force in x-direction

F_a = amplitude of the oscillating wave drift force

F_d = constant wave drift force

$F(\omega)$ = Fourier transform of $f(t)$

$F_H(\omega)$ = Fourier transform of $f_H(t)$

$f(t)$ = arbitrary signal

$f_H(t)$ = Hilbert transform of $f(t)$

$G(\omega_1,\omega_2)$ = complex quadratic transfer function of wave drift force

$g(\tau_1,\tau_2)$ = quadratic impuls response function of wave drift force

H = depth of the vessel

$H(\omega)$ = transfer function of Hilbert filter

h = water depth

i = $\sqrt{-1}$

k = wave number = $2\pi/\lambda$

k_{yy} = longitudinal gyradius of the vessel

L = length between perpendiculars

m = mass of the tanker

m_{xx} = virtual mass of the tanker

$m_{\zeta 0}$ = area of the wave spectrum

$m_{\zeta 1}$ = first moment of the area of the wave spectrum

N = number of low-frequency surge oscillations in extinction tests or number of wave components

N_x = number of low-frequency surge motion oscillations in tests

$P(\omega_1,\omega_2)$, $Q(\omega_1,\omega_2)$ = components of the quadratic transfer function dependent on ω_1 and ω_2

S_ζ = wave spectrum

$S_{F_x}(\mu)$ = spectral density of the longitudinal wave drift force for frequency μ

$T(\omega_1,\omega_2)$ = amplitude of the quadratic transfer function dependent on ω_1 and ω_2

$\overline{T}_1$ = mean wave period

T = draft of the vessel

T_x = natural period of the moored vessel in x-direction

T_Θ = pitch period of the vessel

T_z = heave period of the vessel

t = time

u_a = amplitude of an oscillation quantity

$\tilde{u}_{a1/3}^+$, $\tilde{u}_{a1/3}^-$ = significant peak, trough value

$u_{a\ max.}^+$, $u_{a\ max.}^-$ = maximum, minimum value

$2\tilde{u}_{a1/3}$ = significant double amplitude

$2u_{a\ max.}$ = maximum double amplitude

x = linear surge displacement

x_N = N^{th} amplitude of the decaying surge motion

$\dot{x}$, $\ddot{x}$ = first and second derivatives of displacement with respect to time

z = linear heave displacement

ε_i = phase angle of the i^{th} wave frequency component

ζ = wave elevation

ζ_a = wave amplitude of a regular wave

ζ_i = wave amplitude of i^{th} wave frequency component

$\tilde{\zeta}_{w1/3}$ = mean of the highest one-third crest-to-trough wave heights.

Θ = pitch motion

λ = wave length

μ = frequency of low-frequency part of the second-order forces

μ_e = natural frequency of the system

σ_x = root-mean square value of the surge motion

τ = time lag

$\omega = 2\pi/T$ = wave frequency

ω_i = i^{th} frequency component

ω_x = = natural frequency of the system

∇ = displacement volume

REFERENCES

1. Maruo, H.: "The Drift of a Body Floating on Waves", Journal of Ship Research, Vol. 4, December 1960.
2. Remery, G.F.M. and Hermans, A.J.: "The Slow Drift Oscillations of a Moored Object in Random Seas", Soc. Pet. Eng. J., June 1972.
3. Pinkster, J.A.: "Mean and Low-frequency Wave Drifting Forces on Floating Structures", Ocean Engineering, October 1979.
4. Wichers, J.E.W. and van Sluijs, M.F.: "The Influence of Waves on the Low-frequency hydrodynamic Coefficients of Moored Vessels", Offshore Technology Conference, Paper OTC 3625, 1979.
5. Tretter, S.A.: "Discrete-time Signal Processing", 1976, John Wiley.
6. Dalzell, J.F.: "The Applicability of the Function Polynomical input-output Model to Ship Resistance in Waves", SIT-DL-75-1794, Davidson Laboratory, Stevens Institute of Technology, January 1975.
7. Pinkster, J.A. and Huijsmans, R.H.M.: "The Low-frequency Motions of a Semi-Submersible in Waves", to be presented at: BOSS '82, Boston.

Designation	Symbol	Unit	200,000 DWT VLCC
Length between perpendiculars	L	m	310.00
Breadth	B	m	47.20
Draft even keel	T	m	18.90
Depth	H	m	28.70
Displacement volume	∇	m^3	234,994
Centre of gravity above keel	$\overline{KG}$	m	13.32
Longitudinal radius of gyration	k_{yy}	m	77.47
Block coefficient	C_B	-	0.850
Midship section coefficient	C_M	-	0.995
Waterline coefficient	C_W	-	0.890
Pitch period	T_θ	sec.	10.2
Heave period	T_z	sec.	11.4

Table 1 - Main particulars of the tanker

Spring constant C_x ton/m	Natural period T_x sec.	Natural frequency ω_x rad./sec.	Total mass m_{xx} ton.sec^2.m^{-1}	Added mass a_{xx} ton.sec^2.m^{-1}	Still water damping b_{oxx} ton.sec.m^{-1}
13.60	270.0	0.023	25113	559	18.0
53.72	136.6	0.046	25388	834	23.4

Table 2 - Experimentally determined data of the system

Wave spectrum			C_x	Analyzed data on measured surge motion				Calculated data according to frequency domain σ_x in m	
No.	$\tilde{\zeta}_{w1/3}$ m	$\overline{T}_1$ sec.	ton.m^{-1}	N_x	σ_x m	$2\tilde{x}_{a1/3}$ m	$2x_{a\ max.}$ m	with wave damping	without wave damping
1	12.33	14.0	13.6	36	9.95	35.83	60.95	11.95	25.15
2	9.45	13.7	13.6	32	8.02	27.69	38.40	8.32	14.49
3	7.61	13.6	13.6	-	-	-	-	5.80	8.79
4	5.16	13.3	13.6	-	-	-	-	3.15	4.01
5	12.50	12.0	13.6	-	-	-	-	13.82	32.32
6	9.85	12.0	13.6	33	11.98	44.43	61.12	10.26	19.87
7	6.01	11.4	13.6	36	4.77	19.53	30.45	4.51	6.46
8	4.86	11.1	13.6	36	2.74	10.36	16.52	3.04	3.95
5	12.50	12.0	53.72	-	-	-	-	5.70	12.02
6	9.85	12.0	53.72	67	3.62	12.77	16.25	4.18	7.39
7	6.01	11.4	53.72	66	1.25	4.78	7.58	1.79	2.42
8	4.86	11.1	53.72	67	0.63	2.22	2.98	1.18	1.47

Table 3 - Review of tests; measured and calculated low-frequency surge motions

In-phase components $P(\omega_1,\omega_2)$

ω_1 \ ω_2	0.08	0.16	0.24	0.32	0.40	0.48	0.56	0.64	0.72	0.80	0.88	0.96	1.04
0.08	0	-1.9	-3.0	-1.5	0.5	-2.2							
0.16		0	-0.6	0	-0.5	-0.3	1.8	0					
0.24			-0.1	1.0	1.7	-1.0	-0.1	-0.1					
0.32				-0.8	2.2	1.0	-3.3	-1.6	-4.4				
0.40					-3.5	2.9	-1.1	-0.6	1.2	-5.8			
0.48						-8.7	3.7	-2.7	1.1	-2.3	-3.9		
0.56							-12.9	-0.2	-3.7	0	-2.7	0.1	
0.64								-11.9	-3.6	1.4	-2.9	-6.9	-2.3
0.72									-8.6	-1.3	2.3	-1.7	-3.2
0.80										-9.2	0	6.1	1.7
0.88											-8.7	-4.3	2.2
0.96												-8.7	-5.2
1.04													-8.8

Out-of-phase components $Q(\omega_1,\omega_2)$

ω_1 \ ω_2	0.08	0.16	0.24	0.32	0.40	0.48	0.56	0.64	0.72	0.80	0.88	0.96	1.04
0.08	0	3.9	3.5	-1.2	0	-1.4							
0.16		0	1.3	0.7	0.3	-1.6	-3.5						
0.24			0	-1.0	0.3	0.2	-4.2	-6.6					
0.32				0	-1.9	1.9	-3.6	-4.8	-9.1				
0.40					0	-4.2	4.6	-3.0	-3.8	-7.7			
0.48						0	-6.4	-0.4	-3.5	-6.4	3.5		
0.56							0	-1.9	-2.3	-3.8	-7.8	5.9	
0.64								0	3.4	-0.6	-10.0	-4.2	5.3
0.72									0	2.9	-2.4	-11.9	-2.7
0.80										0	4.0	0.9	-6.0
0.88											0	3.5	1.2
0.96												0	2.6
1.04													0

Amplitudes $T_{12} = T(\omega_1,\omega_2) = \sqrt{P^2(\omega_1,\omega_2) + Q^2(\omega_1,\omega_2)}$

ω_1 \ ω_2	0.08	0.16	0.24	0.32	0.40	0.48	0.56	0.64	0.72	0.80	0.88	0.96	1.04
0.08	0	4.3	4.6	2.0	0.5	2.6							
0.16		0	1.5	0.7	0.6	1.6	3.9						
0.24			0.1	1.4	1.7	1.0	4.2	6.6					
0.32				0.8	2.9	2.2	4.9	5.0	10.1				
0.40					3.5	5.1	4.7	3.1	4.0	9.6			
0.48						8.7	7.4	2.7	3.7	6.8	5.2		
0.56							12.9	1.9	4.3	3.8	8.2	5.9	
0.64								11.9	4.9	1.5	10.4	8.1	5.7
0.72									8.6	3.2	3.4	12.0	4.2
0.80										9.2	4.0	6.2	6.3
0.88											8.7	5.5	2.5
0.96												8.7	5.8
1.04													8.8

Matrix-values in ton.m^{-2}
Frequencies in rad.sec^{-1}
Water depth 206 m

Table 4 - Quadratic transfer function of longitudinal wave drift force on the tanker in head waves

Wave spectrum			Mean wave damping $\overline{b_{1xx}}$ in ton.sec.m^{-1}	
No.	$\tilde{\zeta}_{w1/3}$ m	$\overline{T}_1$ sec.	Time domain	Frequency domain
1	12.33	14.0	65.52	61.76
2	9.45	13.7	39.09	36.68
3	7.61	13.6	24.76	23.34
4	5.16	13.3	11.71	11.04
5	12.50	12.0	-	80.52
6	9.85	12.0	52.12	49.50
7	6.01	11.4	20.56	19.03
8	4.86	11.1	13.40	12.35

Table 5 - Calculated mean wave damping

Wave spectrum No. 1: $\tilde{\zeta}_{w1/3}$= 12.33 m, $\overline{T}_1$= 14.0 sec. ; Spring constant C_x= 13.6 ton.m^{-1}					
Procedure	σ_x m	$\tilde{x}_{a1/3}^{+}$ m	$x_{a\ max.}^{+}$ m	$\tilde{x}_{a1/3}^{-}$ m	$x_{a\ max.}^{-}$ m
Measured	9.95	14.17	27.32	-24.22	-35.34
Time domain measured wave drift forces					
b_{oxx}	26.98	43.50	67.25	-56.25	-80.08
$b_{oxx} + b_{1xx}(t)$	11.85	11.57	27.56	-23.67	-33.42
Time domain computed wave drift forces					
b_{oxx}	29.76	48.90	62.97	-69.03	-77.60
$b_{oxx} + b_{1xx}(t)$	13.08	16.53	25.37	-35.14	-41.70
$b_{oxx} + \overline{b_{1xx}}$	12.66	14.90	25.65	-35.14	-43.27

Table 6 - Some statistical data on measured and time domain computed low-frequency surge motions

Wave spectrum No.	$S_{F_x}(\mu_e)$ in $ton^2.sec.$ Calculated according to frequency domain	
	μ_e= 0.023 rad./sec.	μ_e= 0.046 rad./sec.
1	98,567	-
2	32,737	-
3	12,057	-
4	2,502	-
5	162,825	115,561
6	61,825	43,665
7	6,513	4,664
8	2,436	1,723

Table 7 - Spectral density of the wave drift force at the natural frequency of the system

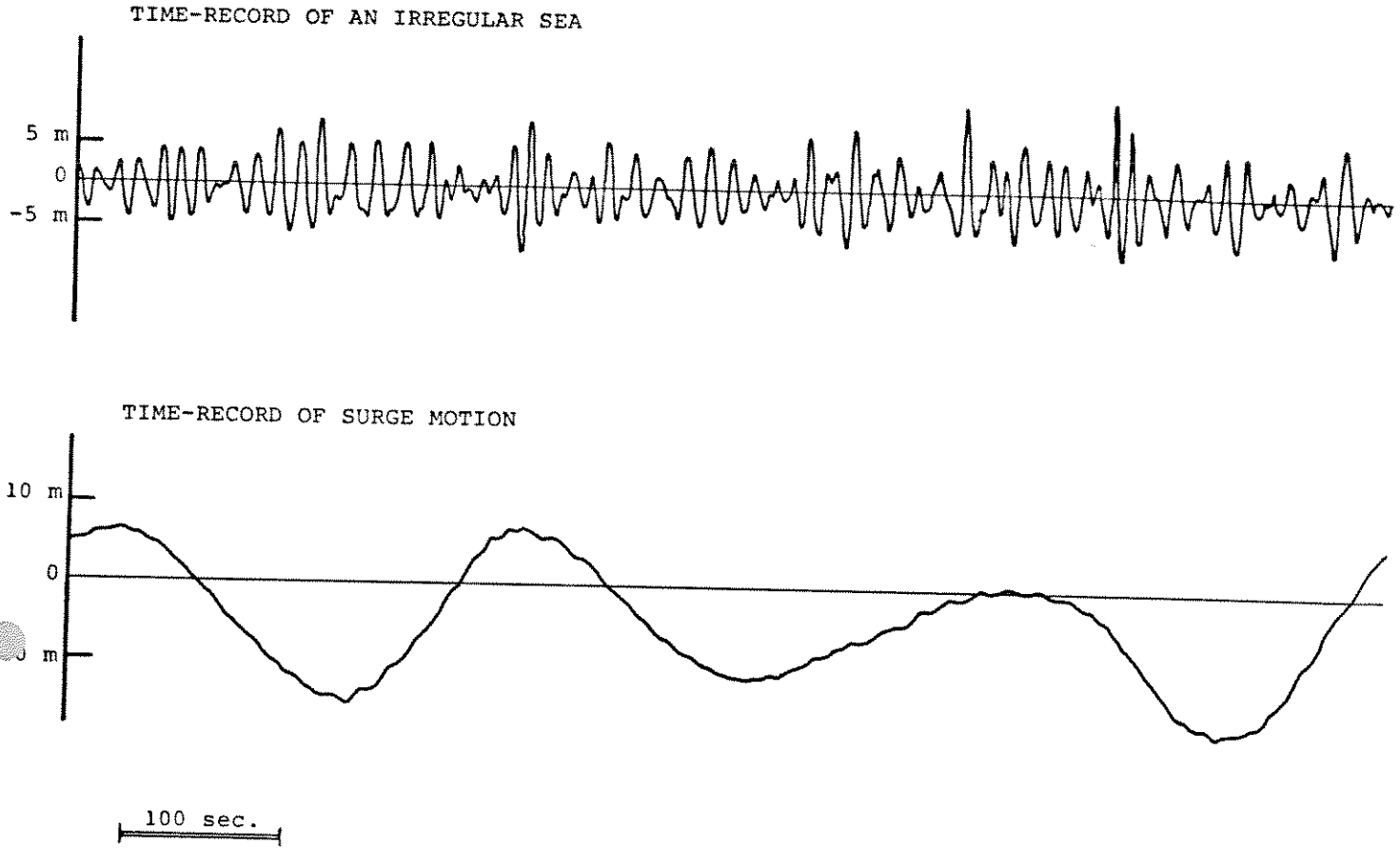

Fig. 1 - Low-frequency surge motion of a moored VLCC

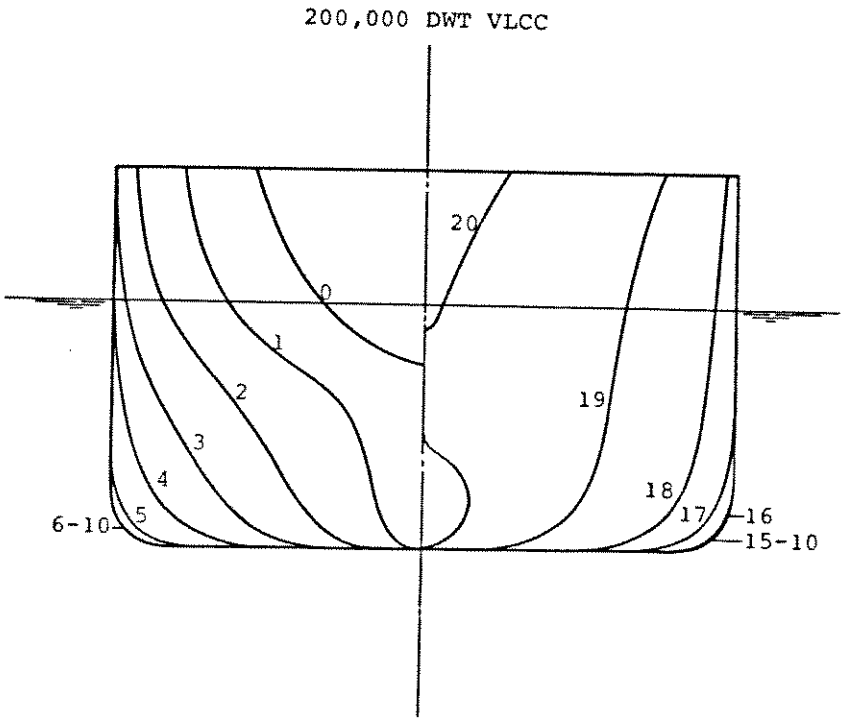

Fig. 2 - Body plan of the tanker

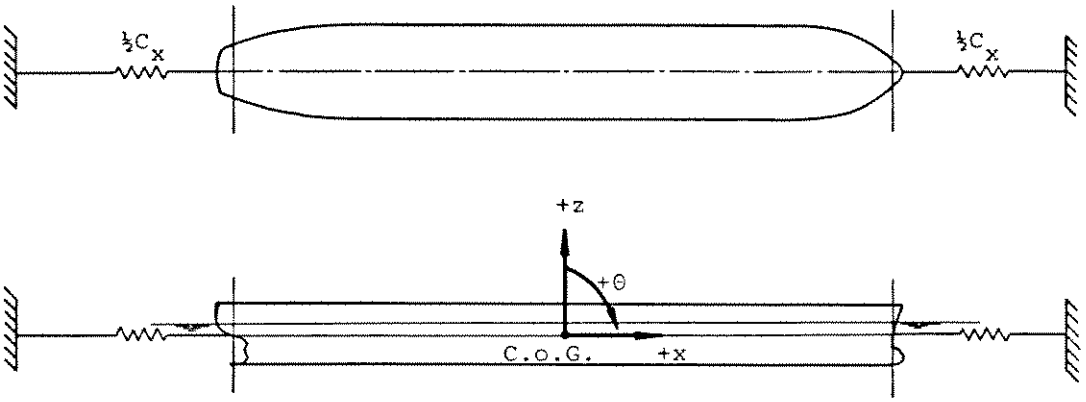

Fig. 3 - Test set-up

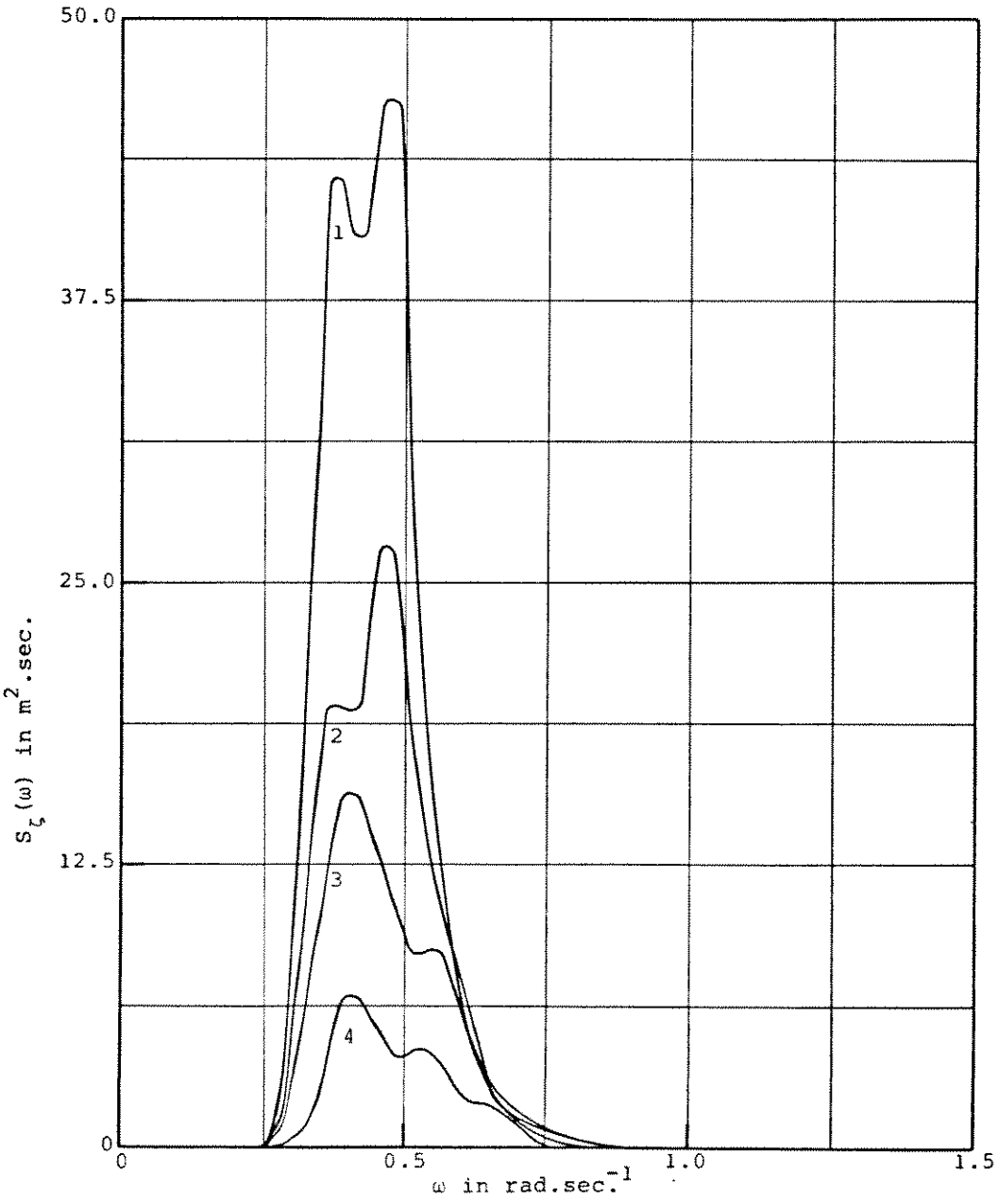

Fig. 4a - Spectral densities of the wave spectra

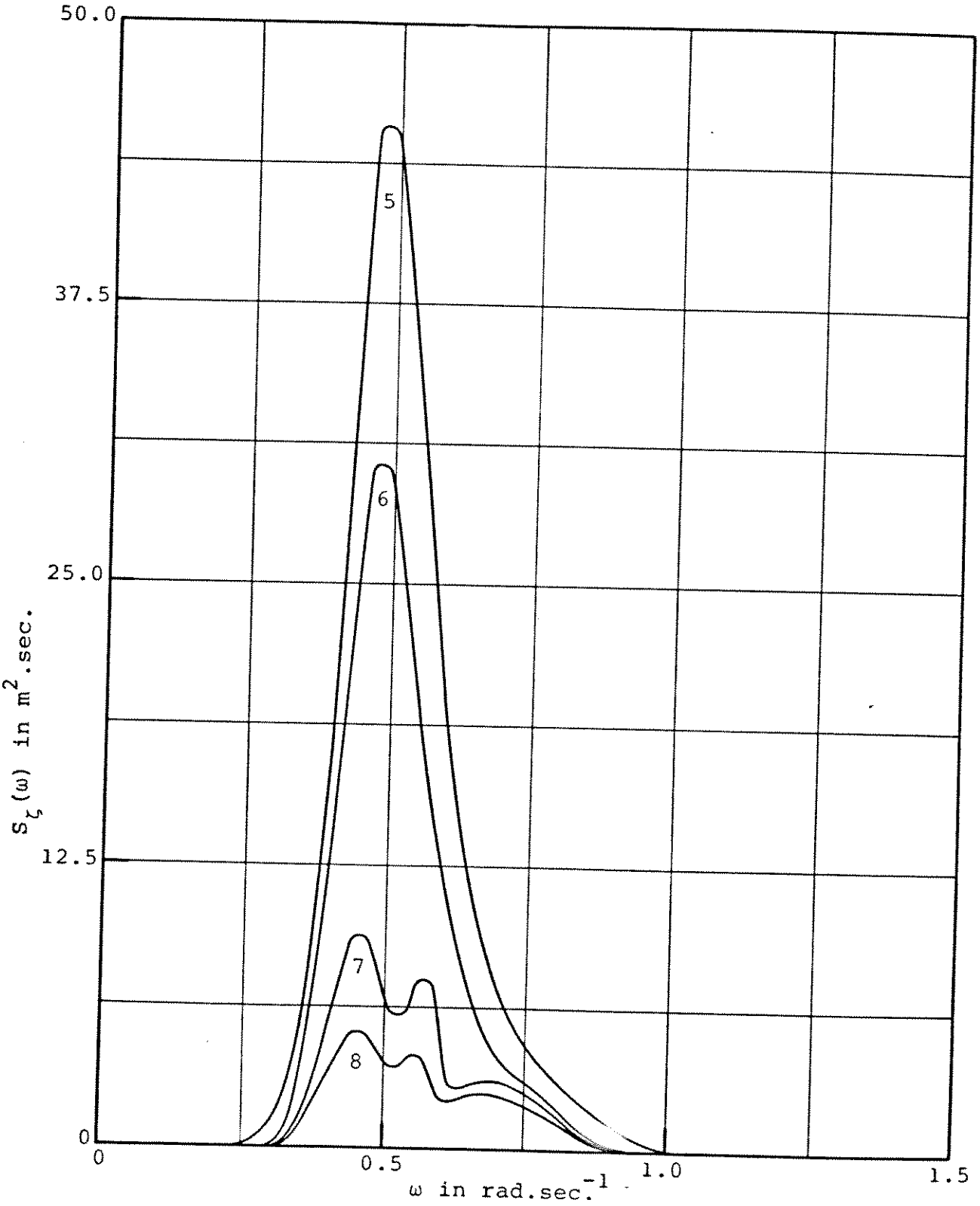

Fig. 4b - Spectral densities of the wave spectra

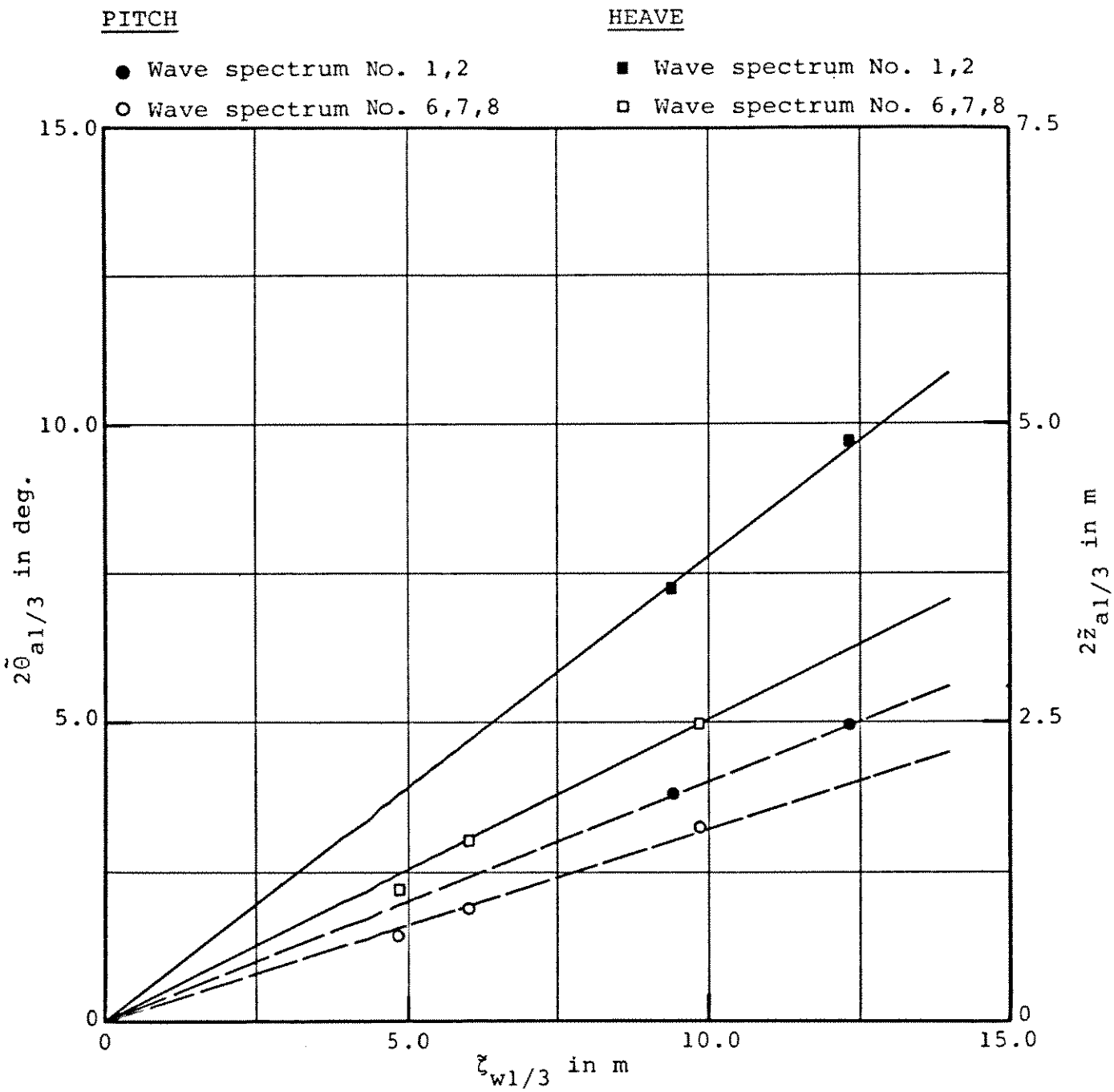

Fig. 5 - Measured significant pitch and heave motions versus significant wave height

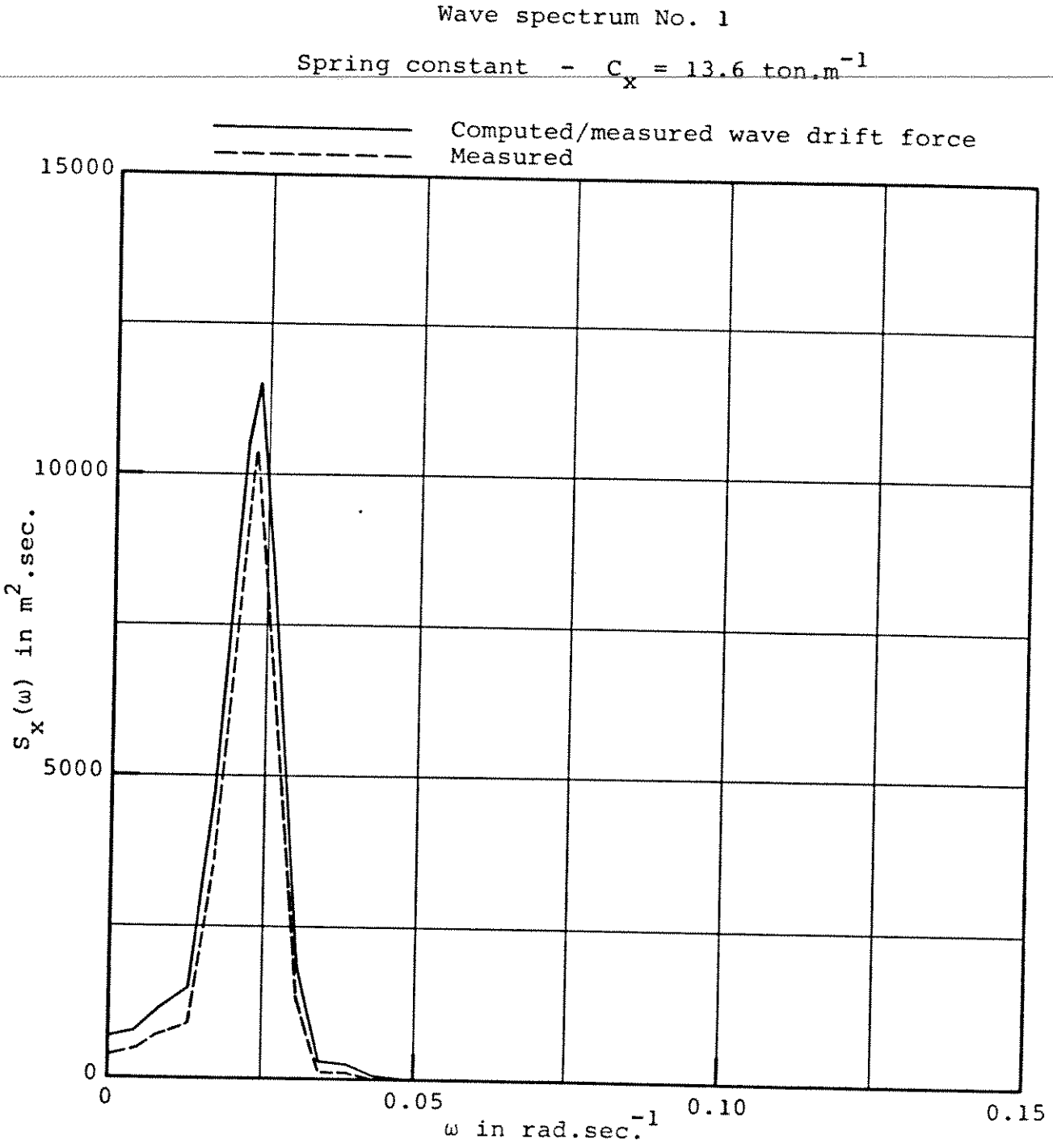

Fig. 6 - Spectra of the measured and computed surge motion

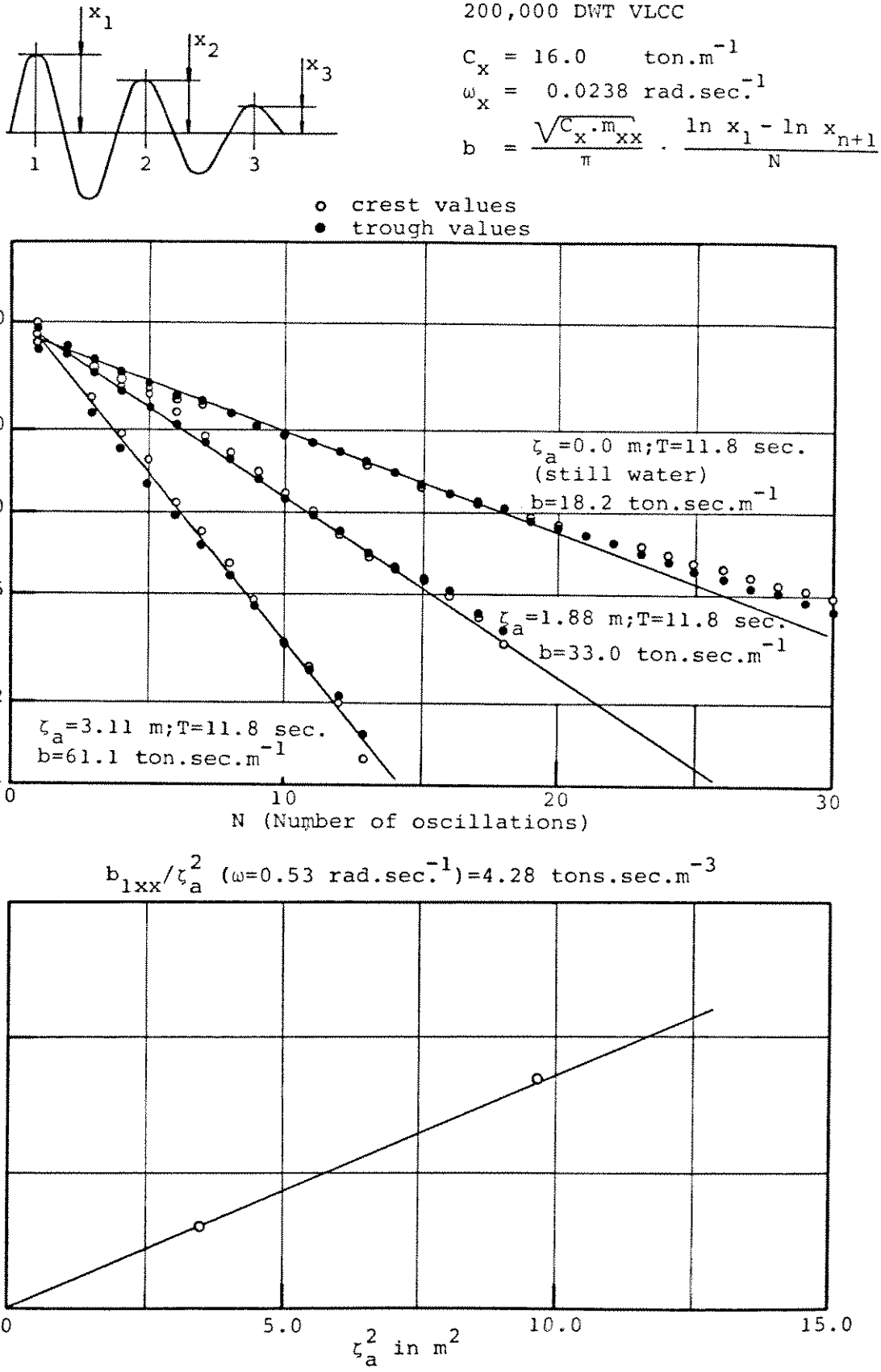

Fig. 7 - An example of the wave damping experimentally determined by extinction tests

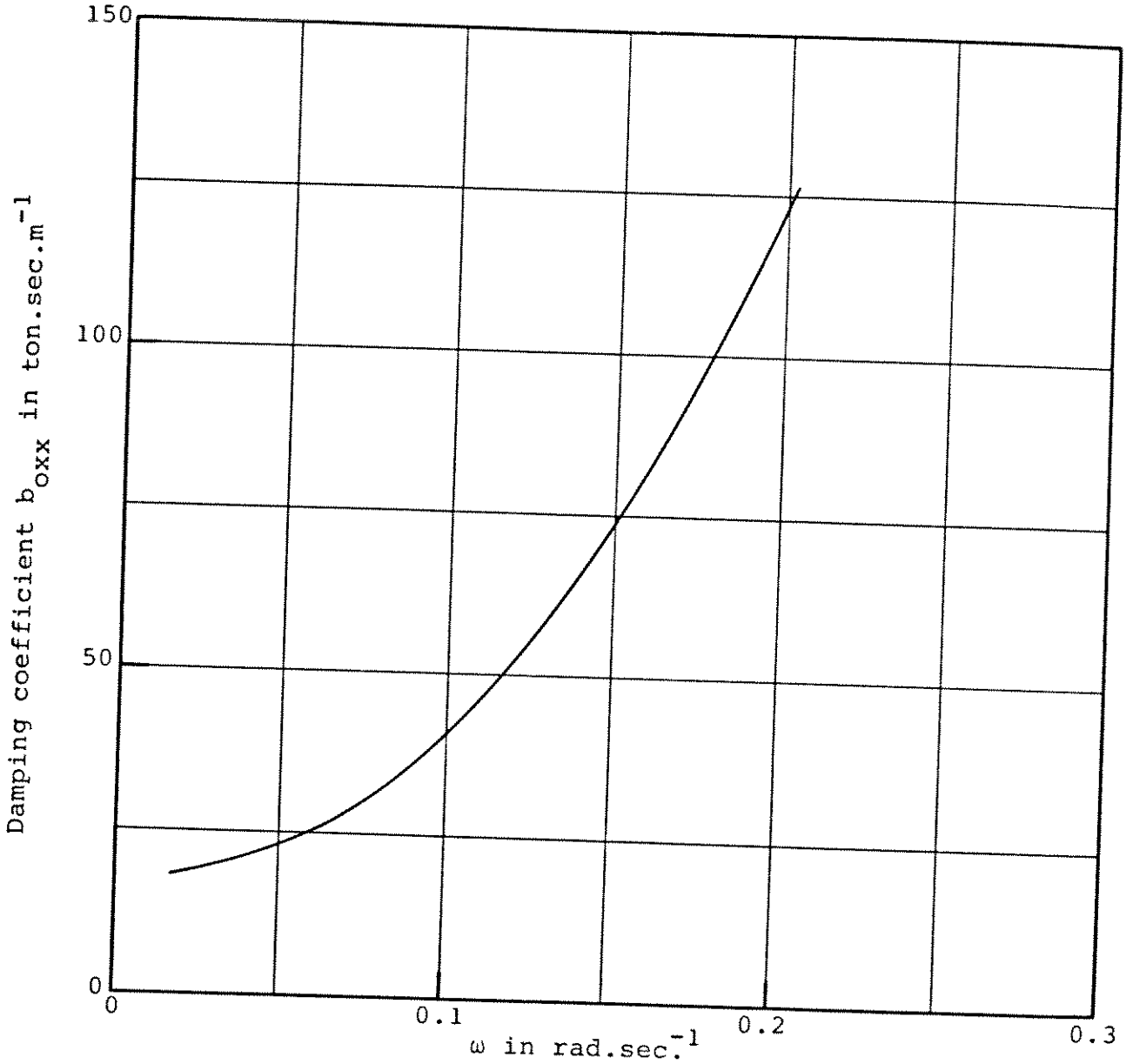

Fig. 8 - Measured still water damping coefficient (ref. [4])

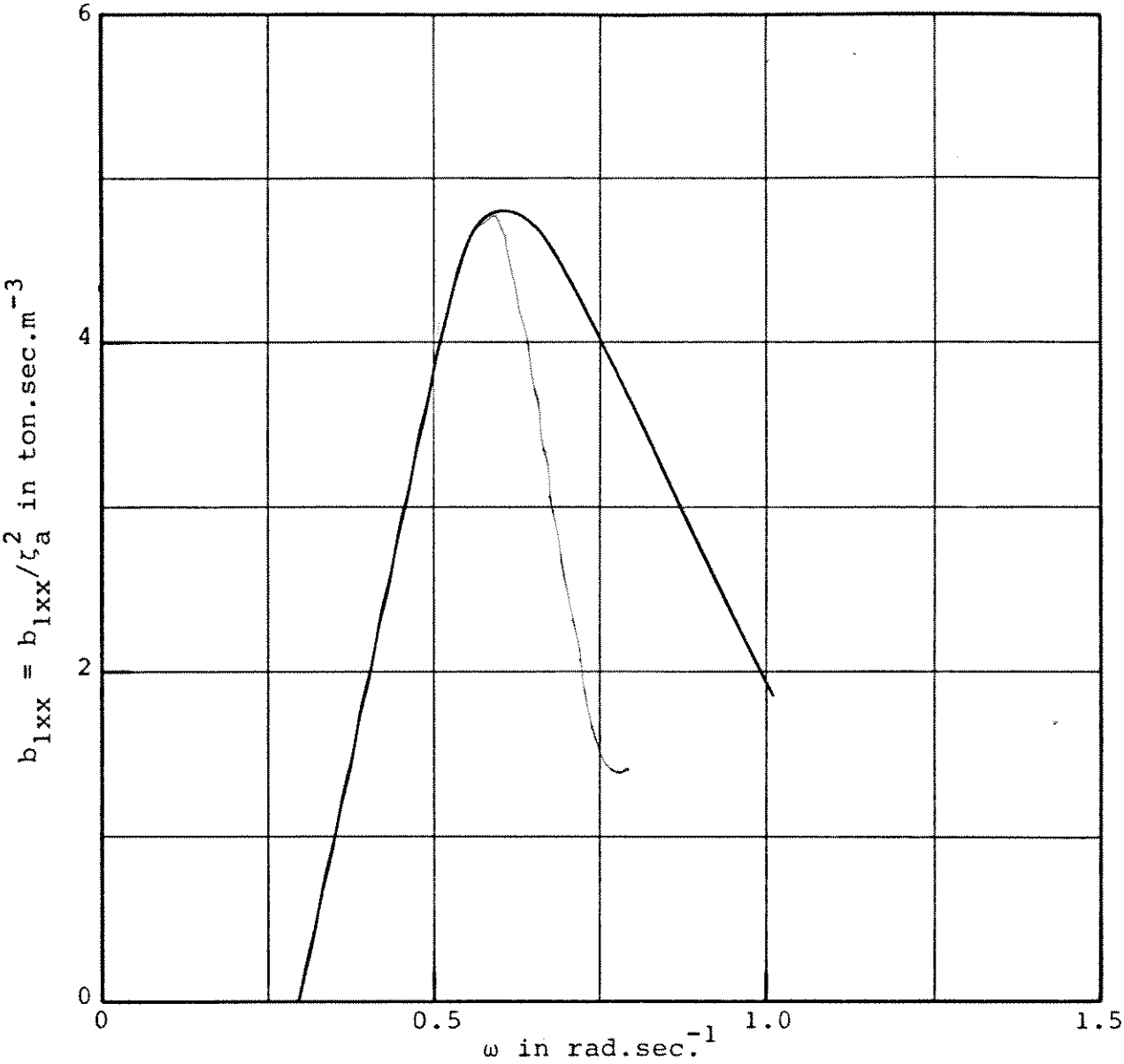

Fig. 9 - Measured quadratic transfer function of the wave damping (ref. [4])

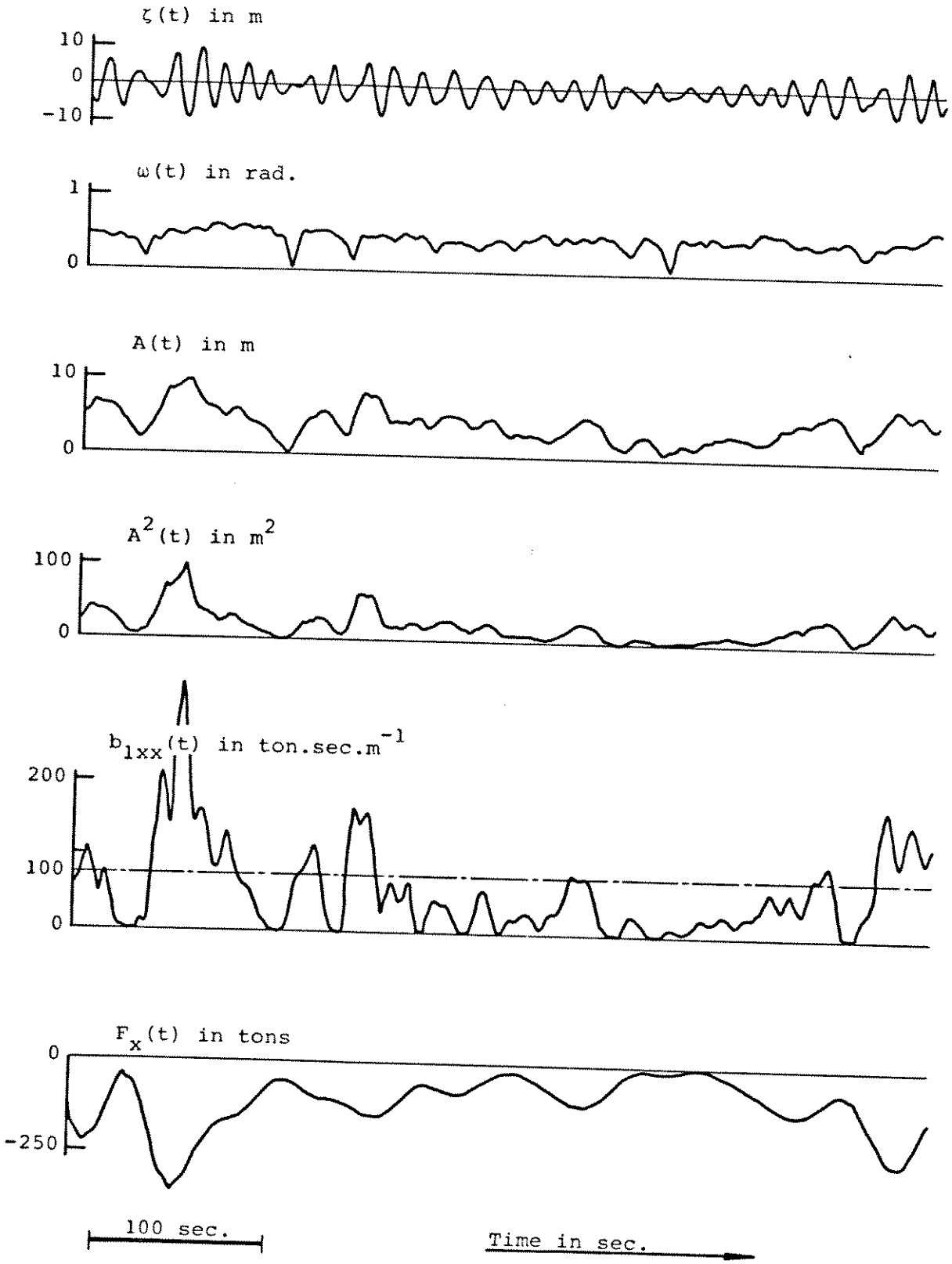

Fig. 10 - Time domain computation of wave damping coefficient and wave drift force derived from the time record of the adjusted waves

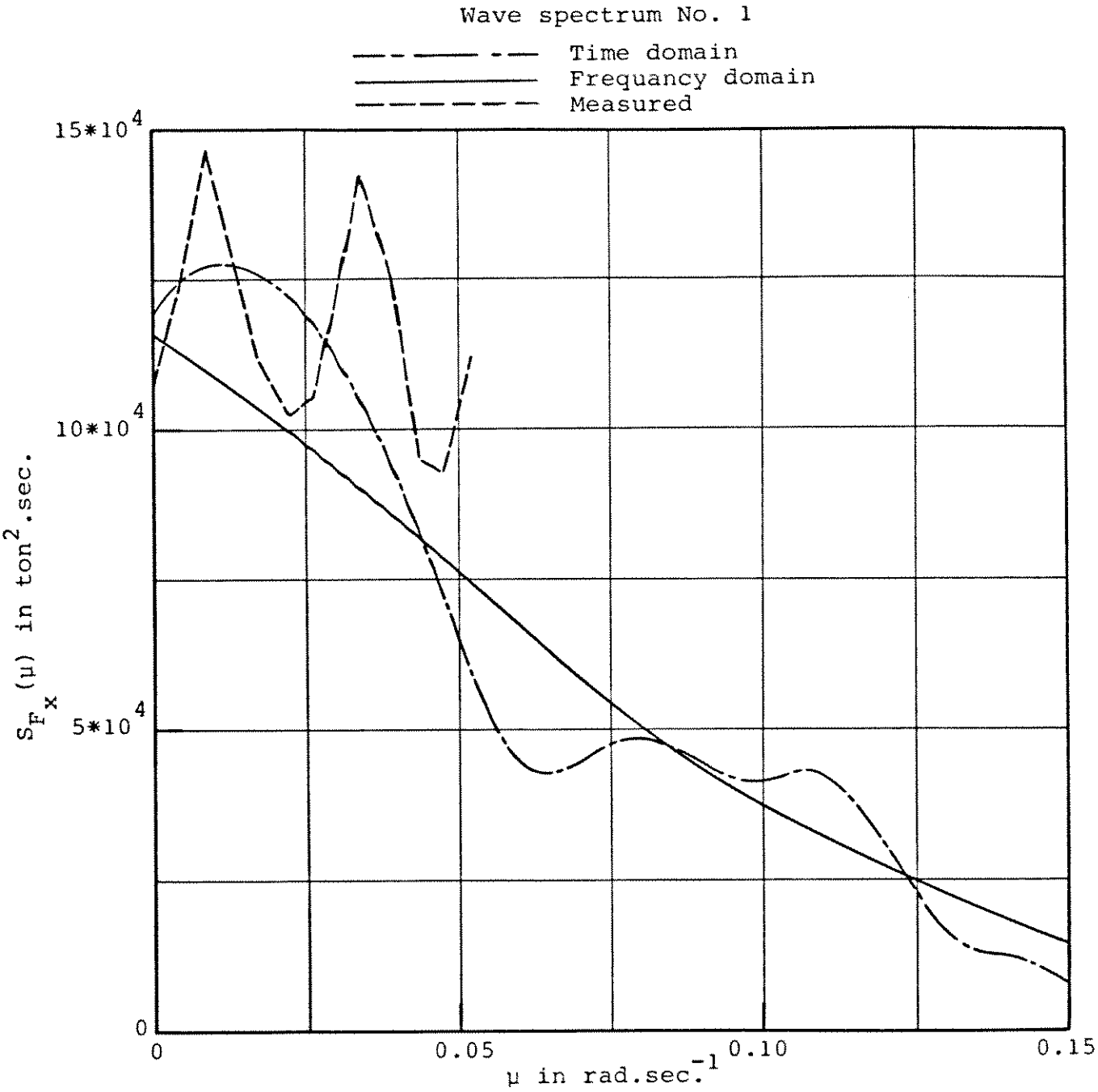

Fig. 11 - Spectral density of the measured and computed lonitudinal wave drift forces

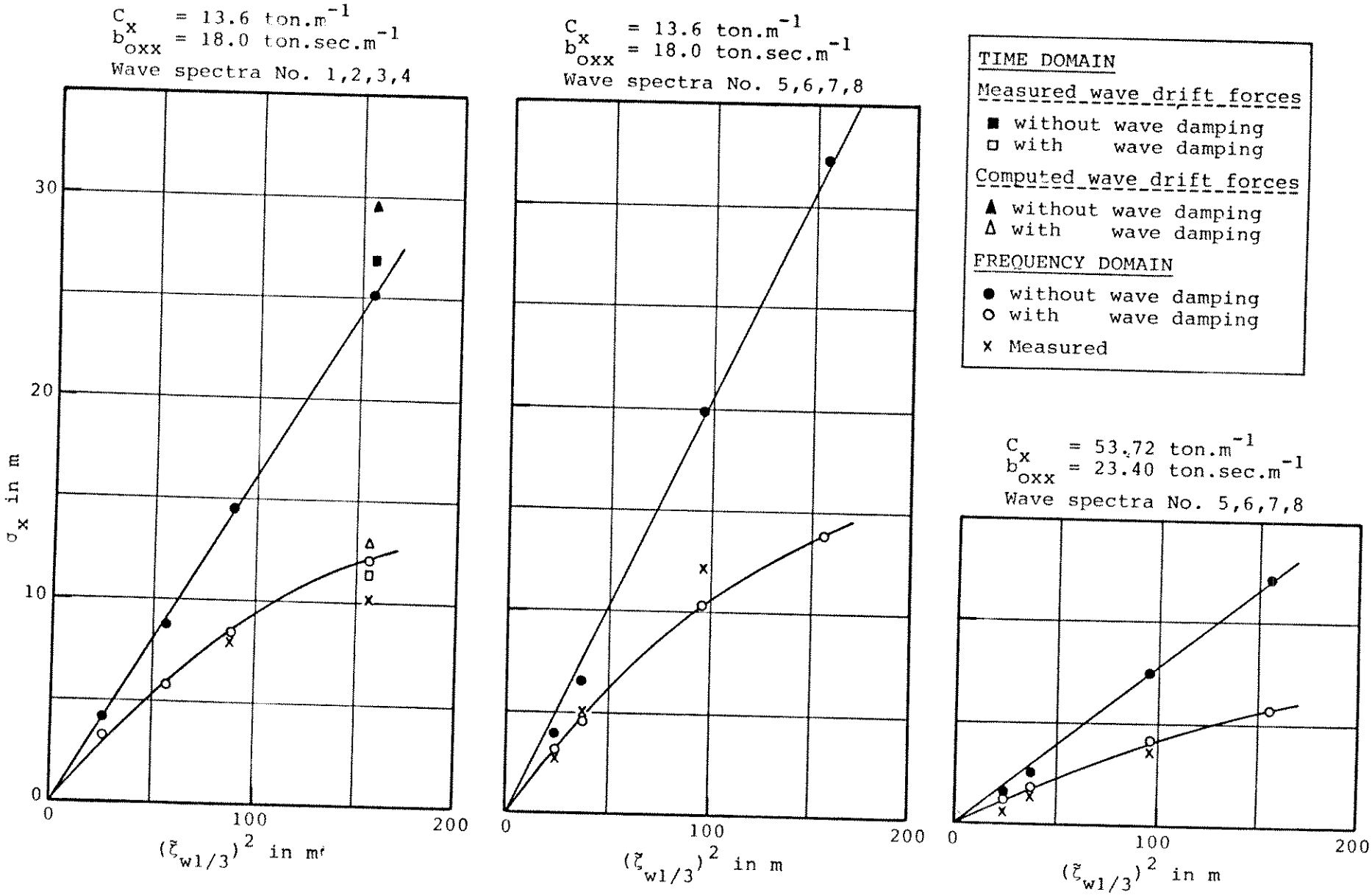

Fig. 12 - Root-mean square values of the low-frequency surge motions versus significant wave heights squared